agriculture

MDPI

Article

Pear Tree Growth Simulation and Soil Moisture Assessment Considering Pruning

Chengkun Wang [1], Nannan Zhang [1,2], Mingzhe Li [1], Li Li [1] and Tiecheng Bai [1,2,*]

[1] School of Information Engineering, Tarim University, Alaer 843300, China
[2] Southern Xinjiang Research Center for Information Technology in Agriculture, Tarim University, Alaer 843300, China
* Correspondence: baitiecheng@taru.edu.cn

Abstract: Few studies deal with the application of crop growth models to fruit trees. This research focuses on simulating the growth process, yield and soil moisture assessment of pear trees, considering pruning with a modified WOrld FOod Studies (WOFOST) model. Field trials (eight pruning treatments) were conducted in pear orchards in Alaer and Awat in Xinjiang, China and data were measured to calibrate and evaluate the modified model. In two pear orchards, the simulated total dry weight of storage organs (TWSO) and leaf area index (LAI) were in good agreement with the field measurements of each pruning intensity treatment, indicating that the R^2 values of TWSO ranged from 0.899 to 0.976, and the R^2 values of LAI ranged from 0.849 to 0.924. The modified model also showed high accuracy, with a normalized root mean square error (NRMSE) ranging from 12.19% to 26.11% for TWSO, and the NRMSE values for LAI were less than 10%. The modified model also had a good simulation performance for the soil moisture (SM) under all eight pruning intensity treatments, showing good agreement ($0.703 \leq R^2 \leq 0.878$) and low error (NRMSE $\leq$ 7.47%). The measured and simulated results of different pruning intensities showed that the highest yield of pear trees was achieved when the pruning intensity was about 20%, and the yield increased and then decreased with the increase in pruning intensity. In conclusion, the modified WOFOST model can better describe the effects of summer pruning on pear tree growth, yield and soil moisture than the unmodified model, providing a promising quantitative analysis method for the numerical simulation and soil moisture assessment of fruit tree growth.

Keywords: pear tree; grow simulation; yield assessment; pruning; soil moisture

Citation: Wang, C.; Zhang, N.; Li, M.; Li, L.; Bai, T. Pear Tree Growth Simulation and Soil Moisture Assessment Considering Pruning. *Agriculture* **2022**, *12*, 1653. https://doi.org/10.3390/agriculture12101653

Academic Editor: Peter A. Roussos

Received: 27 August 2022
Accepted: 3 October 2022
Published: 9 October 2022

1. Introduction

Pear (*Pyrus* spp.) tree is a deciduous tree of Rosaceae native to China, which was cultivated and planted about 3300 years ago [1]. In recent years, the research on pear trees mainly focused on the effects of a water deficit on mature pear trees [2], the leaf physiological responses of mature pear trees to regulated deficit irrigation [3], the effects of different fertilization times on pear trees [4], and the effect of different N fertilizer applications on pear trees [5]. However, few studies have focused on pear tree growth description and pear orchard yield estimation using a growth model.

Perennial fruit trees greatly differ from annual field crops in terms of their physiology and management. With the increase in tree age, the fruit tree canopy will continue to expand, and the branches and leaves will vigorously grow [6]. Pruning is an important horticultural practice that generally promotes vegetative growth. Nutritional growth characteristics after pruning are influenced by the intensity and severity of pruning [7]. This activity is important for improving fruit quality and yield [8,9]. Pruning can also affect the distribution of solar radiation in the canopy [10]. Solar radiation plays an irreplaceable role in the entire growth and development cycle of plants [11,12], especially in the form of sugar and the accumulation of dry matter [13]. To improve fruit quality during harvest,

many researchers have been attempting to improve the utilization of solar radiation [14]. Therefore, optimal photosynthetically active radiation (PAR) is critical to stimulating the photosynthetic process. Summer pruning improves canopy structure and solar radiation interception through the canopy [12,15], as well as improving PAR distribution in the canopy [16,17]. At the same time, pruning regulates the natural ratio of nutrition to reproductive plant growth [18], increases airflow through the canopy, improves the soil water balance [19], and stimulates vegetative growth [7].

The crop growth model is a mathematical model that quantifies crop growth processes, looking at physiological and ecological principles [20–22]. These models simulate biomass growth and yield formation by simulating plants' major physiological activities, such as photosynthesis, gas exchange between the canopy and atmosphere, phenology, and external natural environments, such as soil moisture and temperature dynamics, to predict the evolution of crops, from seeding to harvest [23,24]. Meteorological parameters, such as short-wave radiation, wind speed, temperature, precipitation, etc., are important inputs for these models [25]. Through the efforts of related researchers, crop growth models have been greatly improved. At first, models could only simulate a certain physiological process of an individual crop; at present, they can simulate the entire crop growth process. Crop models have also been combined with multidisciplinary approaches, yielding fruitful results [23,26]. Many crop growth models have been developed to simulate the growth of different crops in different regions, such as Decision Support Systems for Agrotechnology Transfer (DSSAT) [27], The Strategic Training Initiative in Community Supervision (STICS) [28], crop-water productivity model (AquaCrop) [29], WOrld FOod Studies (WOFOST) [30], MOdel for NItrogen and Carbon in Agroecosystems (MONCIA) [31] and Agricultural Production Systems Simulator (APSIM) [32]. Each of these models has its own features and areas of expertise. These models are widely used in annual crops including wheat [33], maize [34], rice [35], potato [36] and cotton [37]. These crop models are constantly being innovated and developed to provide better advice for decision-making in farm crop management [30]. For example, the WOFOST model has been in use for the last 25 years and is continuously updated to increase its applications [30], the EPIC model is used to reduce the impact of climate change on agriculture [38], the APSIM model is used to provide early warnings of drought yield reduction in maize [39], and the the STICS soil-crop model is used for large-scale assessment to reduce nitrate leaching in temperate conditions [40]. However, apart from previous studies on jujube growth simulation [41], few studies have applied crop growth models to fruit trees.

The WOFOST model is a mechanical growth model that depicts plant growth in terms of light energy allocation and CO_2 assimilation as growth-driving processes, and crop phenology development as a growth-controlling process [42]. The WOFOST model takes one day as a time step to estimate leaf area index, aboveground biomass and the storage organ biomass of crops [43]. The model demonstrates crop growth, development and eventual yield, from seedling emergence to maturity [44]. The WOFOST model has been widely used in regional yield estimation and response to crop and environmental changes [45–47].

Although WOFOST has significantly contributed to the simulation of various agricultural management and ecological environments, it was mostly applied to annual crops and not to perennial fruit trees such as fruit trees. Additionally, there are no studies that consider the effects of summer pruning when using crop models, and there are no crop models specifically designed to deal with the effects of summer pruning on fruit tree growth. Therefore, the application of the crop model to research the effects of summer pruning on the growth and developmental status of pear trees and the integrated changes in pear trees under different pruning intensities is promising.

In this study, the objectives are as follows: (a) to modify the WOFOST model to simulate pear tree growth and soil moisture considering pruning, (b) to calibrate the crop parameters and validate the performance of the improved model, (c) to describe the response of yield and leaf area index (LAI) to different pruning intensities, (d) to explore

the feasibility of using the modified crop growth model for the numerical simulation of pear tree growth.

2. Materials and Methods

2.1. Field Experiments Design

In this study, the city of Alaer in southwestern China was chosen as the experimental site because of its large and concentrated pear cultivation area. Field trials and data collection were conducted in the pear orchard (81°01′02″ E, 40°33′14″ N) in Alaer city, as shown in Figure 1. Meanwhile, a pear orchard (80°28′12″ E, 40°35′36″ N) in the Awat area was selected for data collection and used to verify the model performance. The two pear orchards were about 65 km apart. The climate of the entire region is typical of an arid warm–temperate climate, and annual rainfall is usually less than 100 mm. The annual total evaporation is about 2400 mm. The frost-free period is between 178 and 220 days. The annual average temperature ranges from 11.2 to 13.1 °C. The lowest temperature month is January, and the annual ≥10 °C accumulated temperature is 3450–4432 °C. The average daily sunshine is about 15 h during the main growing period of pear trees. The soil type of pear orchard is sandy loam. The soil has good permeability, and the groundwater depth is below 3 m. Some of the physical and chemical properties of the soils are shown in Appendix A (Table A1).

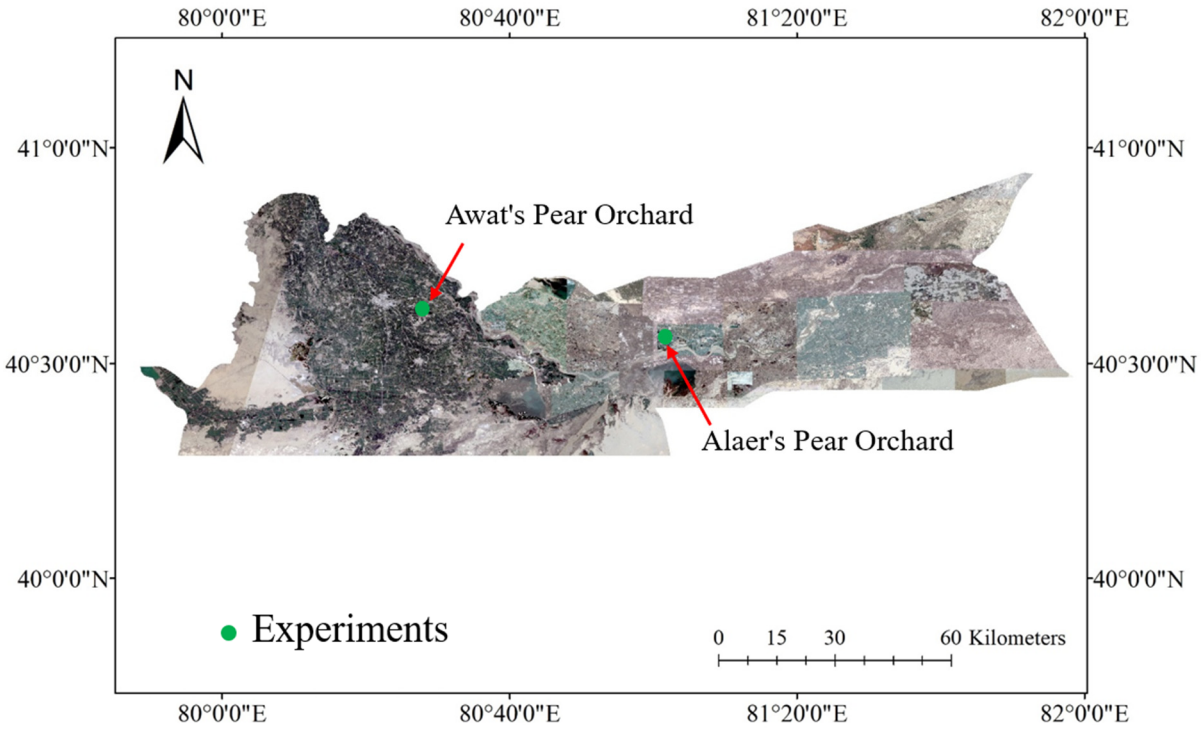

Figure 1. The location of experimental orchards in Alaer (81°01′02″ E, 40°33′14″ N) and Awat (80°28′12″ E, 40°35′36″ N), Xinjiang, China.

The pear trees in the two orchards were eight years old (*CV* Korla) and reached a high yield age. The soil of the two orchards had similar physical and chemical properties (see Table A1) and planting density. The spacing between rows in the orchard was 4 m × 3 m. The uniform pear tree growth area was selected to divide the test plot. Pear trees broke buds in early spring and reach peaked biomass in late August. Fruits were harvested in late August or early September.

Fertilization and irrigation were performed based on local experience values. A total of 300 kg ha^{-1} of pure nitrogen (N), 390 kg ha^{-1} of phosphorus pentoxide (P_2O_5) and 200 kg ha^{-1} of potassium oxide (K_2O) was fertilized into the soil five times. The irrigation

was 300 mm and occurred about 8 times (from early April to early August). Irrigation was applied at days of the year (DOY) = 108, 121, 136, 148, 161, 176, 198 and 212, respectively. Summer pruning for the Alaer pear orchard took place on 5 June 2021 and, for the Awat pear orchard, on 9 June 2021. All pear tree pruning methods were similar, and mainly took place to control the total length of new tips, retain fruit branches, and remove nutrient branches and stunted fruit. Local pear orchard traditional pruning intensity was about 20%, and usually less than 35%. Therefore, eight treatments were designed, and the pruning intensity was set to unpruning, 5% pruning, 10% pruning, 15% pruning, 20% pruning, and 25% pruning, 30% pruning and 35% pruning.

The shape of the pear tree is shown in Figure 2. The pear tree was a dwarf, densely planted Korla pear, with a large crown at the bottom and a small crown at the top, and an elongated spindle-shaped tree. The tree's morphological characteristics were characterized by similar lateral branches growing uniformly on the central trunk, with a height of about 3.8 m, stem height 2.8~3.5 m, and crown diameter 0.9~3.8 m. There were about 21 (between 18 and 24) lateral branches of the pear tree, which were pruned into three layers. There were about 7 branches in the lower layer (110~180 cm in length), 8 branches in the middle layer (80~110 cm in length), and 6 branches in the upper layer (40~80 cm in length).

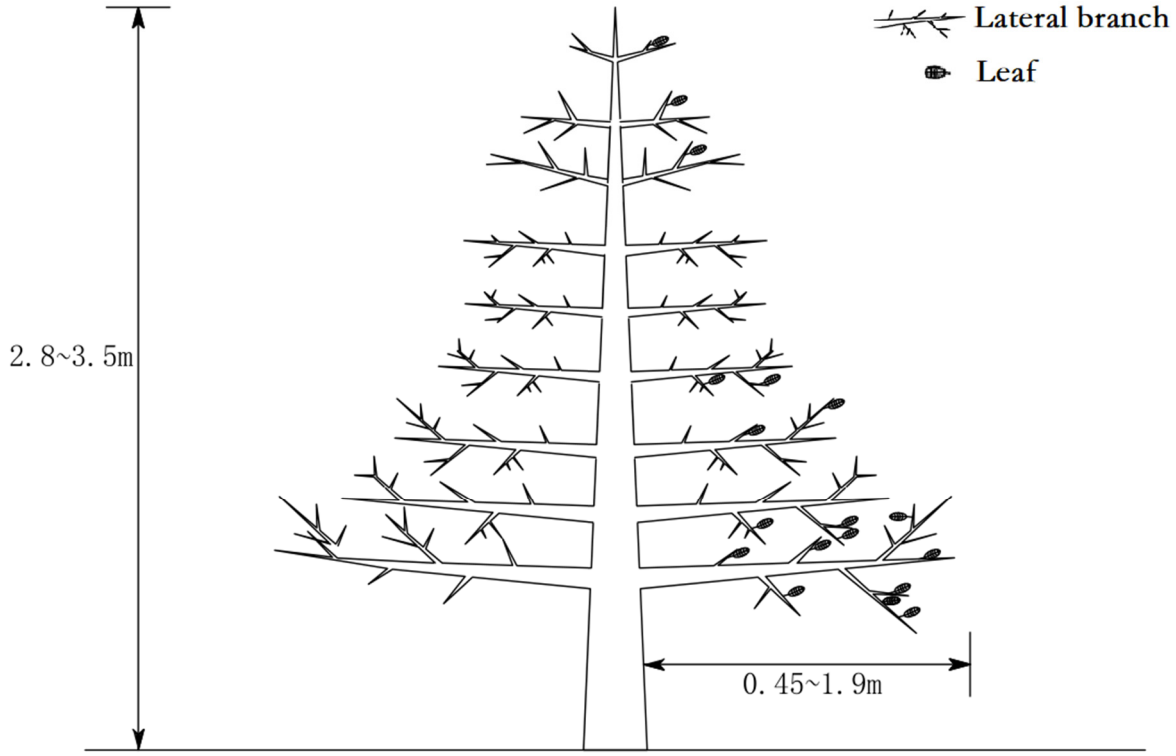

Figure 2. Schematic description of the shape of the experimental pear tree.

2.2. Field Data Measurements and Observation

Based on a modified WOFOST model, calibration and verification data were used to simulate water-limited pear growth. The WOFOST model requires input from daily meteorological data and crop parameters, soil parameters and agricultural management parameters [48]. Some parameter acquisition methods referred to previous studies [49]. In the pear orchard of Alaer, the following data were observed and measured to calibrate the model. In Awat, only yield, leaf area index and soil water content were measured in the pear orchard to verify the accuracy of the improved model. The main observation and measurement data were as follows:

- Phenology time: To calibrate the simulation performance of phenological parameters, emergence (leaf blade starts to unfold), flowering (fruit begins to develop), and maturity dates (dry weight of fruit is not increasing) were observed during the growing period. The variation in the time series of the main fertility stages of Korla pear is shown in Figure 3.

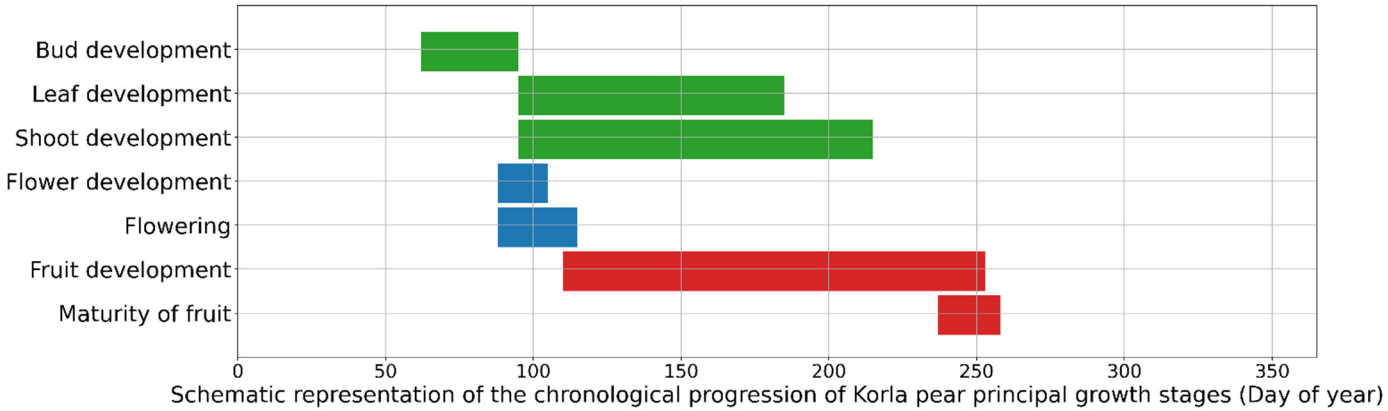

Figure 3. Main development stages of Kolar pear (day of year).

- Initial total dry weight (TDWI): Measurements of the initial buds were used to calculate the TDWI.
- Dry weight: The dry matter mass of leaves and fruits was measured about 13 times during the growth cycle, as shown in Figure 4a. The phenotypic parameters (length, diameter, etc.) of the branches were measured at different periods, and then the density of branches with different diameters was measured (as shown in Figure 4b) to calculate the dry matter of the stems. A number of fruits and leaves were collected at each treatment, dried and treated, and then statistically converted with the observed data to obtain the dry matter mass of each treatment. After fruit harvest, leaf drop nets were placed to collect leaves from the whole tree, as shown in Figure 4c.
- Canopy structure parameters: LAI and diffuse visible light extinction coefficient of the experimental area were measured about 10 times, especially before and after pruning pear trees, and specific leaf area parameters were measured to obtain diffuse visible light extinction coefficients and verify the performance of simulated LAI.
- Photosynthesis (CO_2 assimilation) parameters: Parameters such as net photosynthetic rate was measured with an LI-COR 6400XT instrument (LI-COR, United States). Maximum CO_2 assimilation rate and light-use efficiency parameters at optimal developmental temperature were obtained by calculation. Leaf area index (LAI), photosynthetically effective intercepted radiation and corresponding radiation abatement coefficients were measured nondestructively twice a week throughout the growth cycle using a plant canopy analyzer (LI-COR LAI-2000).
- Soil moisture content: The sampled soil at every 20 cm (0~100 cm) was brought back to the laboratory and weighed after drying at 85 °C to a constant weight to calculate soil moisture. The field water-holding capacity and soil-water content in saturated conditions were measured using the cutting ring method before seedling emergence. The undisturbed soil was collected at the experimental site and brought back to the laboratory, and the soil-water content was saturated under the conditions of manual intervention. The soil-water content of the undisturbed soil at this time was measured as the saturated soil water content. If the undisturbed soil saturated with water content was placed on top of the air-dried soil, so that the air-dried soil absorbed the gravitational water in the undisturbed soil, then the undisturbed soil water content was measured at this time, to obtain the field water-holding capacity.

Figure 4. (**a**) Field data acquisition such as biomass collection, phenological observations and pruning measurements; (**b**) measurement of stems of different diameters; (**c**) collecting all fallen leaves after harvesting.

- Yield: To evaluate the simulated yield, the weight of all pears from each tree was measured at harvest and the total dry weight of the pears was calculated from the pears' measured water content.
- Agromanagement actions: Irrigation, fertilization and pruning times of pear orchards were observed and recorded.
- Removed biomass was collected and weighed: After summer pruning, all removed stems, fruits and leaves were collected from each test area. They were dried in a forced-air oven at 105 °C for 30 min and then at 85 °C to a constant weight, after which all samples were weighed.
- Weather data: Small weather stations in the pear orchard were used to collect the meteorological input parameters required by WOFOST model. Figure 5 shows the daily maximum and minimum temperature (daily average temperature 12.3~28.7 °C), daily total precipitation and radiation during the main growth period of pear trees in two orchards. The daily minimum and maximum temperatures showed a tendency to rise and then fall, and the daily temperature difference was large. The annual rainfall in the study area was less than 100 mm. The water needs of pear trees mainly depended on irrigation. Although most of the rainfall occurred in summer, the amount of rainfall was very small. The total daily radiation of the two pear orchards was strong, which was conducive to plants' photosynthesis.

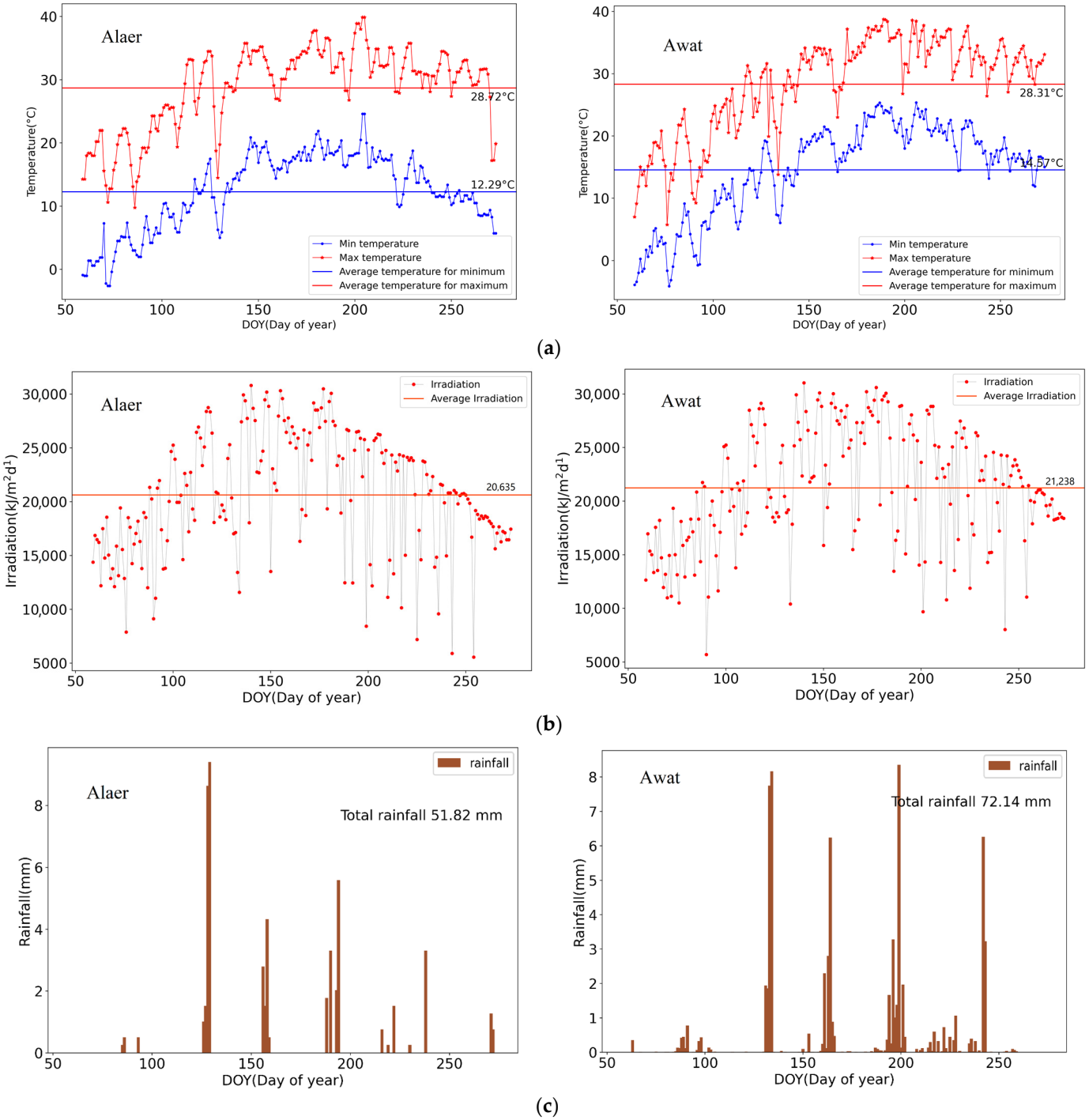

Figure 5. (**a**) Daily minimum and maximum temperature from March to October in Alaer and Awat; (**b**) daily total irradiation from March to October. (DOY: day of year); (**c**) daily total rainfall from March to October.

2.3. Modification of WOFOST Model

This research caused modifications in a WOFOST model called Python Crop Simulation Environment (PCSE) (https://pcse.readthedocs.io/en/stable/, accessed on 6 March 2021). PCSE is a WOFOST model developed using Python. The combination of WOFOST and the Python interpreter provides great system flexibility for model modification. The process of crop growth, dry matter distribution and water transport can refer to the existing

literature [42]. In this study, we mainly improved the model on the basis of considering pruning, as follows:

In pre-exponential crop growth, the growth curve is exponential, and the exponential growth rate of the leaf area index is assumed to be continuous until the source-limited growth of the leaf area index is equal to the exponential growth rate [42]. The leaf area index growth rate per time step in the pre-exponential growth phase can be seen in Equation (1). During the exponential growth stage, the accumulated leaf area index at time step t is calculated; see Equation (2):

$$L_{Exp,t} = LAI_t RLT_e \quad (1)$$

$$LAI_t = LAI_{t-1} + L_{Exp,t}\Delta t \quad (2)$$

where $L_{Exp,t}$ represents the growth rate of the leaf area index at time step t during the exponential growth stage (ha ha^{-1} d^{-1}); LAI_t represents leaf area index at time step t (ha ha^{-1}); RL represents maximum relative increase in leaf area index (C^{-1} d^{-1}); T_e represents daily effective temperature (number of degrees above the base temperature for leave ageing) (C) [50]; Δt represents time step (t).

During the development of the pear tree, leaf area expansion is increasingly restricted by the assimilate supply (i.e., source limited increase). In the WOFOST model, it is assumed that the exponential growth rate of the leaf area index will continue until it equals the source-limited growth rate. The growth rate of the leaf area index per time step in the early, exponential growth stage, can be calculated as Equation (3). The accumulated leaf area index at time step t during the exponential growth stage can be described as Equation (4) [42].

$$L_{Sc,t} = \Delta W n_{lv} S_{la} \quad (3)$$

$$LAI_t = LAI_{t-1} + L_{Sc,t}\Delta t \quad (4)$$

where $L_{Sc,i}$ represents the growth rate of the leaf area index at time step t during exponential growth stage (ha ha^{-1} d^{-1}), $\Delta W n_{lv}$ represents net dry matter growth of leaves at time step t (kg ha^{-1} d^{-1}), S_{la} represents specific leaf area at time step t, LAI_t represents leaf area index at time step t (ha ha^{-1}), and Δt represents time step (t).

The net dry matter growth of leaves, $\Delta W n_{lv}$, can be found by subtracting the weight of leaves that died during the current time step from the dry matter growth of leaves, $\Delta W n_{lv}$. The specific leaf area, S_{la} (acronym: SLATB), is defined as the increase in the leaf area of the crop per kg weight increase in the living leaves. LAI_t is initialized by taking the fraction of initial biomass (acronym: TWDI) partitioned to the leaves and multiplying it with the specific leaf area at the current DVS.

To correct for leaf senescence, S_{la} per time step, dry matter weight increases, $\Delta W_{lv,}$ per time step and physiological age page were stored in three different arrays [50]. The arrays were organized as follows: the first element of the array represents the most recent age category (or time step), and the last element of the array represents the oldest age category (or time step) [50]. It should be clear that the position of the element in the array represents its age level in a particular time step [42]. The dry matter weight of dead leaves in the current time step must be determined. The dry matter weight gain from each time step should be subtracted [50]. Therefore, an array contains the net dry matter growth in each time step leaf, ΔW_{lv}.

After adjusting for leaf senescence, cumulative leaf area can be established. The net dry matter weight (ΔW_{lv}) of the remaining and new leaves is multiplied by the specific leaf area [42] (see Equation (3)) to obtain the growth rate of the LAI of living leaves for each age class. Multiplying by delta T and the sum of the classes (Equation (4)) yields the total LAI.

Pruning intensity refers to the percentage of stems, leaves and fruit removed from a single tree during summer pruning. The summer pruning process involves the removal of excess vegetative stems and the removal of poorly developed fruits. Therefore, the pruning of fruit trees is regarded as the unnatural disappearance of branches, leaves and fruits. Only the proportion of branches, leaves and fruits cut during pruning, compared to the

original branches, leaves and fruits, needs to be known. The dry matter weight of the stems (WST), dry matter weight of the storage organs (WSO) and dry matter weight of the leaves (WLV), respectively, should be reduced according to the actual operation. At this point, the dry matter mass of each organ can be calculated by Equation (5)

$$W_{t,i} = (1 - p_i)W_{t-1,i} + \Delta W n_i \Delta t \quad (5)$$

where p_i represents pruning intensity (the default value of p_i *is* 0) and i represents stems (st), roots (rt), leaves (lv). $W_{t,i}$ represents dry matter weight organ i at time step t (kg ha^{-1}).

The leaves removed during summer pruning are new leaves. Combined with the above contents, to calculate the new LAI, the p ratio elements from the array storing leaf information given above are removed. This process can be described by Equations (6) and (7):

$$LAI = LASUM + SAI + PAI \quad (6)$$

$$LASUM = (1 - p) \cdot (LV + SLA) \quad (7)$$

where LAI represents leaf area index, including stem and pod area, SAI represents stem area index and PAI represents pod area index. $LASUM$ represents the sum of LV (kg ha^{-1}), LV represents leaf biomass per leaf class (kg ha^{-1}), SLA represents specific leaf area per leaf class (ha kg^{-1}), and p represents the pruning intensity of leaves.

Among these, the extinction coefficient for diffuse visible light as a function of development stage (KDIFTB) is entered by the user. Measurements were made directly under diffuse reflectance conditions at the early stage of pear tree phenological development, before and after pruning, and during the pre-harvest period, and entered into the crop parameter file; see Table 1.

Table 1. Parameter configuration of KDIFTB at different developmental stages. (DVS: Development Stages).

DVS \ Pruning Intensity	Unpruned	Pruned 5%	Pruned 10%	Pruned 15%	Pruned 20%	Pruned 25%	Pruned 30%	Pruned 35%
DVS = 0.0	0.46	0.46	0.46	0.46	0.46	0.46	0.46	0.46
DVS = 1.260	0.83	0.83	0.83	0.83	0.83	0.83	0.83	0.83
DVS = 1.261	0.83	0.80	0.75	0.72	0.69	0.66	0.63	0.60
DVS = 2.0	0.83	0.83	0.83	0.81	0.79	0.76	0.74	0.71

2.4. Calibration of WOFOST Model

To ensure the accuracy of the model simulation results, the crop model must be calibrated before it can be used in a specific agricultural environment area, and the performance after calibration can be validated [47]. Weather, soil, and crop variables are the primary input parameters for the WOFOST model [30]. In the study, meteorological parameters were directly used from observations from weather stations. Soil parameters were provided from actual field measurements. The crop parameters were obtained using two main methods: calibration of field experimental observations and publicly available data. Specific calibration methods for some parameters can be found in previous studies [49].

2.5. Evaluation of Simulated Performance

The coefficient of determination (R^2) represents the consistency between the measured value and simulated value, root mean square error (RSME) represents the relative error between measured value and simulated value [51], and normalized root mean square error (NRSME) represents the absolute error between measured value and simulated value [52]. NRMSE $\leq$ 10% indicates extremely high accuracy, 10% < NRMSE $\leq$ 20% indicates high accuracy, 20% < NRMSE $\leq$ 30% indicates medium accuracy, and NRMSE > 30% indicates low accuracy [49]. At the same time, the ratio of performance to deviation (RPD) was used as another evaluation index of the model's prediction effect [53]. If the RPD value is greater

than 2, the model has good predictive power and is considered sufficient for analytical purposes [54]. Their values were calculated by Equations (8)–(11).

$$R^2 = 1 - \frac{\sum_{i=1}^{n}(y_i - \widetilde{y_i})^2}{\sum_{i=1}^{n}(y_i - \overline{y_i})^2} \quad (8)$$

$$RMSE = \sqrt{\frac{\sum_{i=1}^{n}(\widetilde{y_i} - y_i)^2}{n}} \quad (9)$$

$$NRMSE = \frac{\sqrt{\frac{\sum_{i=1}^{n}(\widetilde{y_i} - y_i)^2}{n}}}{\overline{y_i}} \quad (10)$$

$$RPD = \frac{SD}{RMSE} \quad (11)$$

where $\widetilde{y_i}$ represents simulated value, y_i represents measured value, $\overline{y_i}$ is average value of the measured values, and n is the number of samples. SD is the standard deviation of the measured values.

3. Results

3.1. Calibration Performance

Crop parameters were calibrated at 20% empirical pruning intensity in the Alaer pear orchard. The significance of these parameters can be found in a previous study [42]. The main calibrated pear crop parameters are shown in Appendix B (Table A2). The main soil parameters are shown in Appendix B (Table A1).

To accurately estimate the pear yield, we compared the simulation results before and after model modification. The total weight of storage organs (TWSO) was a key indicator of the fruit trees' yield. LAI was chosen as an indicator to evaluate the model-simulated crop growth dynamics. The simulated results of LAI, TWSO and soil moisture (SM)-based on calibration data are expressed in Figures 6 and 7. The results showed that the simulation accuracy of the unmodified model was lower than that of the modified model. Compared with the unmodified simulation result trajectory, the simulation using the modified model improved the simulation accuracy of LAI, while the simulation accuracy of TWSO and SM were slightly improved. The measured values of these three parameters were in good agreement with the simulated values, with a R^2 of 0.927 for LAI, 0.987 for TWSO and 0.894 for SM, respectively. The corrected model also shows high accuracy, with an RMSE of 0.13 ha ha^{-1}, 269.17 kg ha^{-1} and 0.01 cm^3 cm^{-3} for LAI, TWSO and SM, respectively. All RPD values were greater than 2, indicating that the modified model had good pear tree growth and soil moisture simulation ability.

3.1.1. Performance of the Unmodified Model

Figure 6 shows a graphical evaluation of the calibration before model modification. The simulated TWSO was in agreement with their field measurements (R^2 = 0.974). The simulated LAI agreed with the measurements at the beginning of the growth cycle, but the summer pruning process could not be simulated by the unmodified model, causing a huge difference in the results (R^2 = 0.495). Similarly, the simulated values of TWSO exactly matched the equivalent measurements at the beginning of the growth cycle. However, the simulated values were slightly lower after summer pruning. LAI was overestimated after the summer pruning in June due to its inability to express the pruning process. For TWSO, it was overestimated from early June to mid-July after pruning and underestimated after mid-July. For SM, most samples were slightly underestimated.

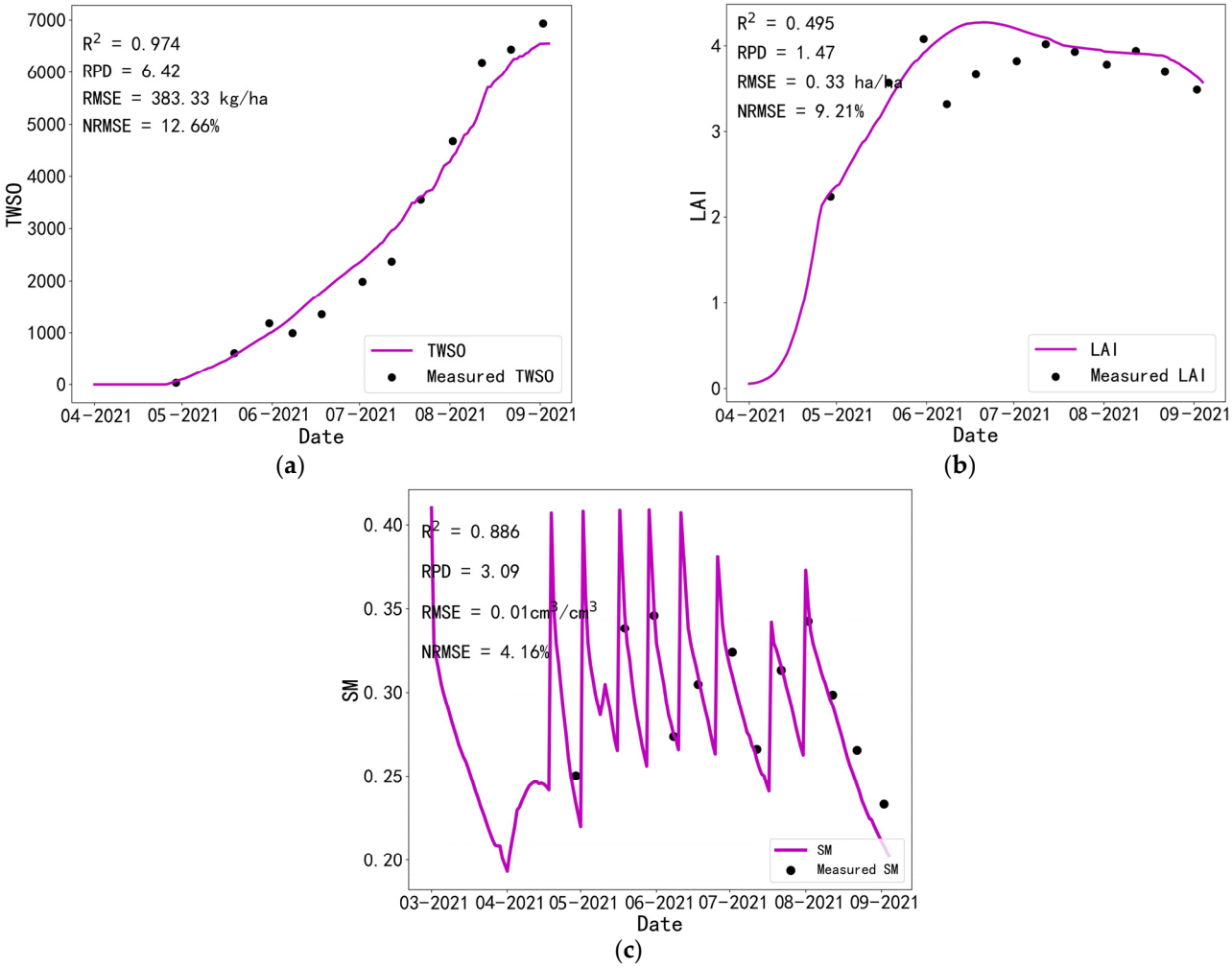

Figure 6. Simulated and measured TWSO (**a**), LAI (**b**) and SM (**c**) based on the unmodified WOFOST model.

3.1.2. Performance of the Modified Model

The simulation results of the improved model are shown in Figure 7. For TWSO, the simulated results before pruning were in high agreement with the measured values. After pruning, the simulated values of TWSO were higher than the actual measured values from early June to mid-July and lower than the actual measured values in late July. After late July, some of the simulated results were in a slightly underestimated state. For LAI, the simulated results before pruning were comparable to the actual measured values, but the simulated results were lower than the actual measured values for a short period after pruning. LAI hardly changed after leaf development ceased. For SM, the simulated value at the end of the growing period is slightly lower than the measured value.

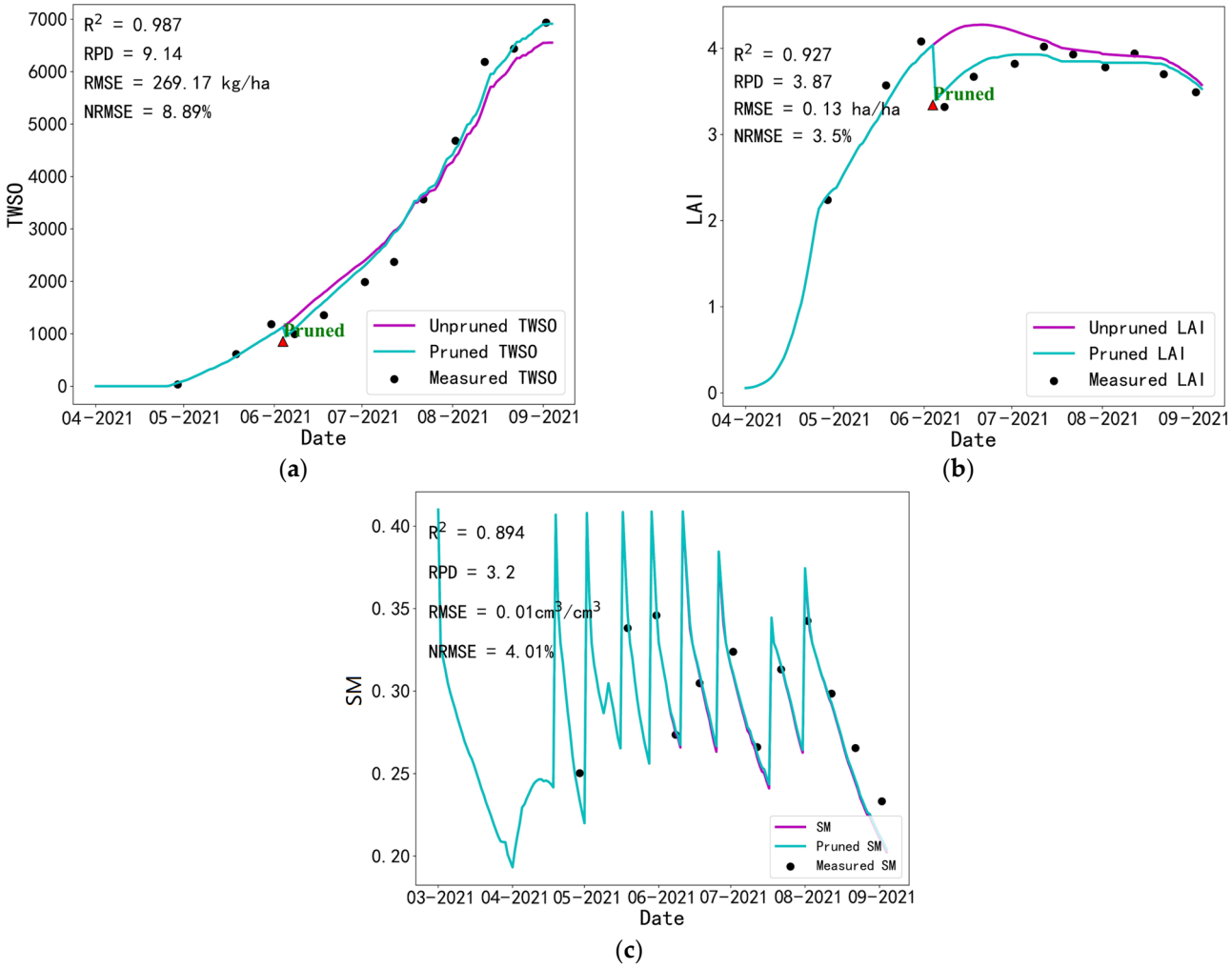

Figure 7. Simulated and measured TWSO (**a**), LAI (**b**) and SM (**c**) based on the modified WOFOST model.

As can be seen from Figure 7, LAI changes were most obvious when orchard pruning was carried out in early June, because, at this time, the leaves were at the end of growth and the generation efficiency of new leaves was low. After July, leaves almost stopped growing. Summer pruning had the least effect on the fruit, because, at this time the fruit was in a slow expansion stage, the weight of individual fruit was smaller and the removal of young fruit in a poor state of growth helped to improve the quality of the rest of the fruit.

Several evaluation indexes of the model were used to ensure that the unmodified model had a satisfactory overall performance in simulating pear tree growth. However, the simulation performance of soil water content (SM) was slightly worse. The simulation results based on the unmodified model showed that LAI simulation was in good agreement with the actual measurement trend at the early growth stage, and the value was slightly overestimated after pruning (Figure 6b). Similarly, TWSO was simulated well in the early growth stage, while the simulated values were lower than the measured values in the late growth stage (Figure 6a). The modified model can simulate LAI, TWSO and SM dynamics during the main growing period. These results provided preliminary evidence that pruning can be accurately modeling when simulating fruit tree growth. Note that the modified model underestimated TWSO values at late stages of fruit growth and development, but this underestimation was acceptable considering the simulation accuracy of the overall results. Compared with the unmodified model, the modified model showed a better simulation performance.

3.2. Validation and Evaluation

3.2.1. Performance of the Simulated TWSO and LAI Growth Dynamics

Pear orchard data obtained from seven pruning treatments of Alaer and eight pruning treatments of Awat were used to validate the simulated TWSO and LAI performance. The simulated dynamics of TWSO and LAI under different pruning intensity treatments were validated for the first time. The performance of the simulated TWSO and LAI before and after the modifications is shown in Tables 2 and 3, respectively. The modified model showed good TWSO simulation performance. The R^2 values of simulated versus measured TWSO based on the unmodified model ranged from 0.784 to 0.973, and the R^2 values of TWSO based on the modified model ranged from 0.899 to 0.976. The NRMSE of the unmodified model for TWSO ranged from 12.95 to 35.01%, and the NRMSE of the modified model ranged from 12.19 to 26.11%, which indicated that the modified model had a better TWSO simulation accuracy than the unmodified model. The results showed that the simulated values of TWSO were in good compliance with the actual measured values, and the performance of the modified model was better than that of the unmodified model. The agreement between simulated and measured LAI based on the unmodified model was higher when the pruning density was less than 15%, and lower when the pruning density was increased. The reason for this may be that the unmodified model does not simulate the changes in LAI after pruning well. The improved model showed good agreement with R^2 values from 0.849 to 0.924. The results also showed that the modified model had high LAI simulation accuracy, with NRMSE values ranging from 3.42% to 8.60%. In the pear orchard at Awat, the simulation accuracy of TWSO at a pruning intensity of 25% and the simulation accuracy of LAI at a pruning intensity of 35% performed poorly compared to other pruning treatments.

Table 2. Simulated TWSO validation for different treatments.

Region	Pruning Intensity	Unmodified Model			Modified Model		
		R^2	RMSE (kg ha^{-1})	NRMSE (%)	R^2	RMSE (kg ha^{-1})	NRMSE (%)
Alaer	0%	0.969	408.69	14.07	0.969	408.69	14.07
	5%	0.973	385.39	12.95	0.976	362.69	12.19
	10%	0.965	450.18	15.30	0.972	401.41	13.64
	15%	0.964	455.65	15.45	0.975	376.99	12.78
	25%	0.948	564.28	19.51	0.968	438.73	15.17
	30%	0.921	636.73	23.83	0.955	479.15	17.93
	35%	0.917	630.65	24.17	0.956	458.92	17.59
Awat	0%	0.945	429.45	18.22	0.945	429.45	18.22
	5%	0.939	438.87	17.37	0.943	428.09	16.94
	10%	0.948	402.04	17.19	0.959	357.23	15.27
	15%	0.92	514.36	20.72	0.939	449.65	18.11
	20%	0.941	424.48	18.93	0.964	329.45	14.69
	25%	0.839	630.16	32.90	0.899	500.10	26.11
	30%	0.910	476.98	23.78	0.948	360.83	17.99
	35%	0.784	650.80	35.01	0.919	399.29	21.48

Table 3. Simulated LAI validation for different treatments.

Region	Pruning Intensity	Unmodified Model			Modified Model		
		R^2	RMSE (ha ha^{-1})	NRMSE (%)	R^2	RMSE (ha ha^{-1})	NRMSE (%)
Alaer	0%	0.924	0.13	3.42	0.924	0.13	3.42
	5%	0.903	0.15	3.99	0.908	0.15	3.90
	10%	0.875	0.18	4.70	0.914	0.15	3.88
	15%	0.882	0.17	4.12	0.911	0.16	3.96
	25%	−1.919	0.71	21.93	0.904	0.13	3.99
	30%	−4.248	1.32	47.37	0.885	0.19	7.01
	35%	−5.209	1.57	62.92	0.905	0.19	7.77
Awat	0%	0.899	0.21	5.44	0.899	0.21	5.44
	5%	0.884	0.22	5.56	0.903	0.20	5.08
	10%	0.852	0.23	5.92	0.920	0.17	4.37
	15%	0.848	0.25	6.45	0.894	0.21	5.38
	20%	0.567	0.36	9.79	0.916	0.16	4.30
	25%	−0.049	0.57	16.94	0.849	0.22	6.42
	30%	−3.077	0.94	30.39	0.868	0.17	5.47
	35%	−4.902	1.46	55.76	0.860	0.23	8.60

3.2.2. Performance of the Simulated Soil Moisture

The measured soil water content (SM) of all treatments in two orchards was used to evaluate the soil moisture simulation performance. The model exhibited good overall SM simulation performance, with R^2 values of 0.832 and 0.791 and NRMSE values of 5.41% (Figure 8). The RMSE between measured and simulated values was also relatively small, with 0.02 cm^3 cm^{-3} for Alaer and 0.01 cm^3 cm^{-3} for Awat.

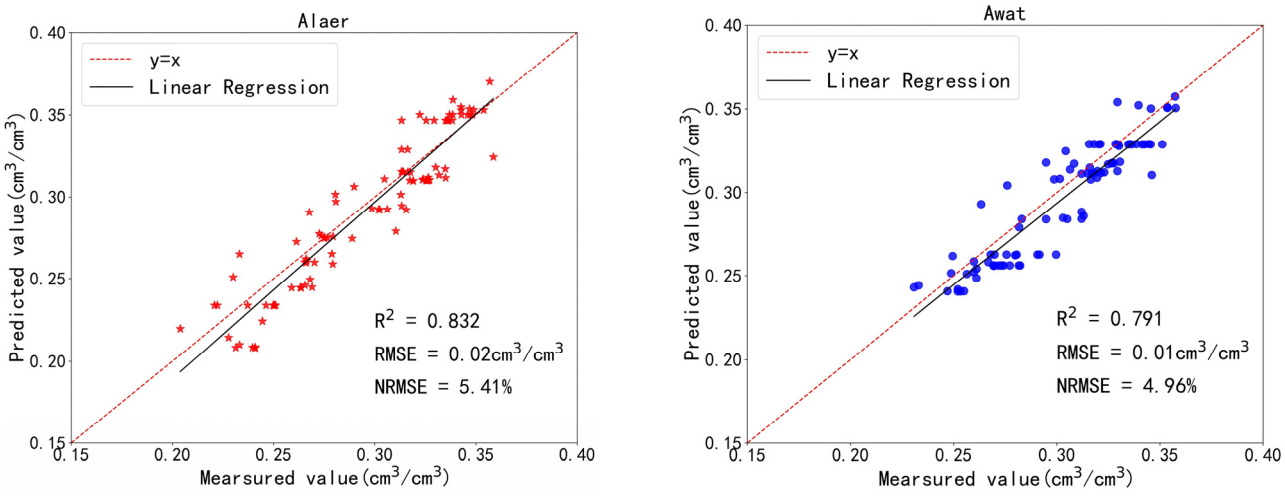

Figure 8. Measured versus simulated soil moisture for different treatments based on modified model.

The local performance of the simulated SM for each trimming treatment is shown in Table 4. The R^2 values of the unmodified model of simulated versus measured SM ranged from 0.369 to 0.878 and the NRMSE values ranged from 4.28 to 8.95%. The modified model simulated SM with R^2 values between 0.703 and 0.878 and NRMSE values between 4.28 and 7.47%. The model modification slightly improved the simulation performance for SM, with better agreement and higher accuracy.

Table 4. Simulated SM Validation for different treatments.

Region	Pruning Intensity	Unmodified Model			Modified Model		
		R^2	RMSE (cm^3 cm^{-3})	NRMSE (%)	R^2	RMSE (cm^3 cm^{-3})	NRMSE (%)
Alaer	0%	0.866	0.011	4.54	0.866	0.011	4.54
	5%	0.878	0.011	4.28	0.878	0.010	4.28
	10%	0.829	0.022	5.03	0.834	0.020	4.99
	15%	0.832	0.021	5.01	0.836	0.018	4.94
	25%	0.791	0.022	5.95	0.827	0.020	5.43
	30%	0.535	0.032	8.95	0.733	0.022	6.79
	35%	0.658	0.029	8.63	0.715	0.021	7.47
Awat	0%	0.779	0.013	4.49	0.779	0.013	4.49
	5%	0.798	0.021	5.15	0.801	0.021	5.14
	10%	0.799	0.010	4.74	0.804	0.010	4.68
	15%	0.743	0.021	5.60	0.767	0.022	5.33
	20%	0.799	0.010	4.64	0.806	0.010	4.56
	25%	0.698	0.021	5.85	0.703	0.020	5.79
	30%	0.626	0.023	5.86	0.763	0.017	4.67
	35%	0.369	0.026	8.77	0.744	0.020	5.59

3.2.3. Performance of the Simulated Final TAGP Based on Modified Model

The final total dry weight of stems, leaves and fruits (TAGP) of all treatments was measured after harvest in both pear orchards and used to assess the simulated performance. The measured and simulated TAGP values are shown in Table 5. The simulated results were in good agreement with the measured results, with deviations ranging from 3.61 to 24.23%. The deviation of TAGP under a 25% pruning intensity treatment in Awat pear orchard and 35% pruning in Alaer was large, but the rest of the treatments performed well (relative error (RE) < 20%), indicating that the modified model can analyze the effect of pruning intensity on TAGP.

Table 5. Simulated and measured values of final TAGP for different treatments based on modified model.

Pruning Intensity	Alaer			Awat		
	Simulated Values (t ha^{-1})	Measured Values (t ha^{-1})	Relative Error (%)	Simulated Values (t ha^{-1})	Measured Values (t ha^{-1})	Relative Error (%)
0%	22.67	24.73	8.33	20.09	18.22	10.25
5%	22.57	20.49	10.14	19.95	22.43	11.04
10%	22.54	19.45	15.91	19.92	21.75	8.39
15%	22.35	23.97	6.77	19.75	17.21	14.76
20%	22.15	21.38	3.61	19.50	18.46	5.65
25%	21.33	18.73	13.90	19.04	15.33	24.23
30%	19.93	22.34	10.79	18.11	16.15	12.11
35%	18.60	15.11	23.07	16.53	14.33	15.33

3.3. Simulated Yield under Different Pruning Intensities Based on Modified Model

The measured yield showed a trend of increasing and then decreasing with the increase in pruning intensity, and the treatment showed the highest yield with 20% pruning intensity; see Figure 9. In comparison, the actual measured pear yields of different treatments in Alaer were higher than those in Awat, which was due to the slightly longer period of pear tree phenological development in Alaer compared to Awat. At the same time, the two pear trees had different daily temperatures at the early stage of phenological development, which affected the flower bud differentiation. During the fruit expansion period, the persistent

high temperatures in Awat reduced the efficiency of canopy photosynthesis, which, in turn, affected the yield.

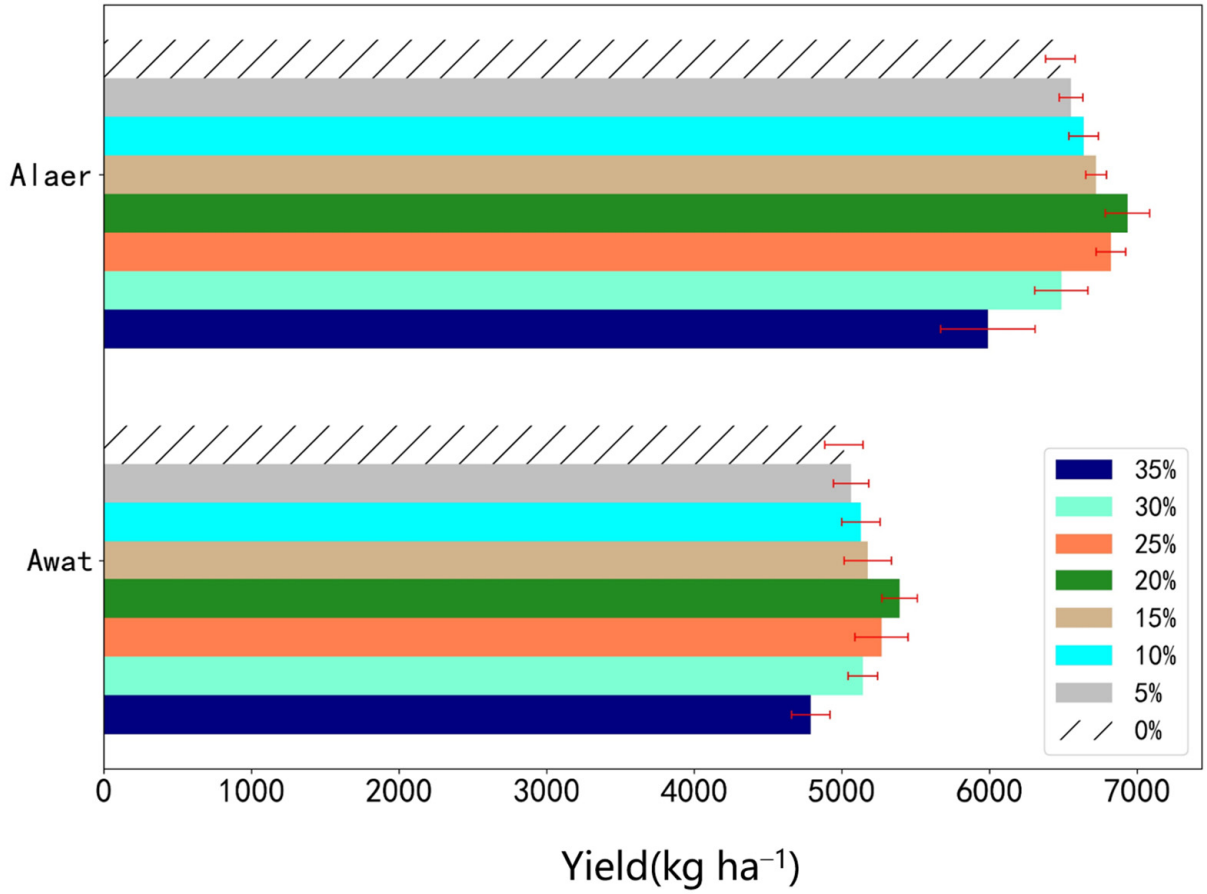

Figure 9. Measured final pear yield for all treatments in Alaer and Awat.

The improved model was used to simulate the yield under different pruning intensities. We set the pruning intensities to unpruned, 5%, 10%, 15%, 20%, 25%, 30%, 35%. The simulated results showed that the effect of pruning intensity on yield first increased and then decreased (Figure 10), and 20% pruning showed the highest yield, which was consistent with the actual observed results (Figure 9). The reason for this may be that the pruning intensity was low, and so a large number of vegetative branches were retained, resulting in less and uneven light exposure in the middle and lower canopy. As the pruning intensity increased, the canopy light condition and the fruit quality were improved. However, when pruning intensity exceeded a certain limit, there was a large reduction in the branches and leaves in the canopy, leading to insufficient dry matter production and lower yield.

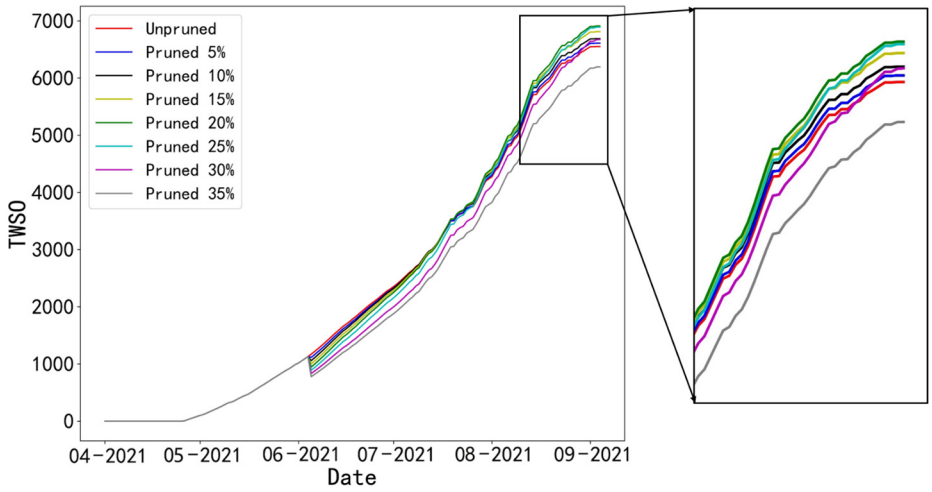

(**a**)

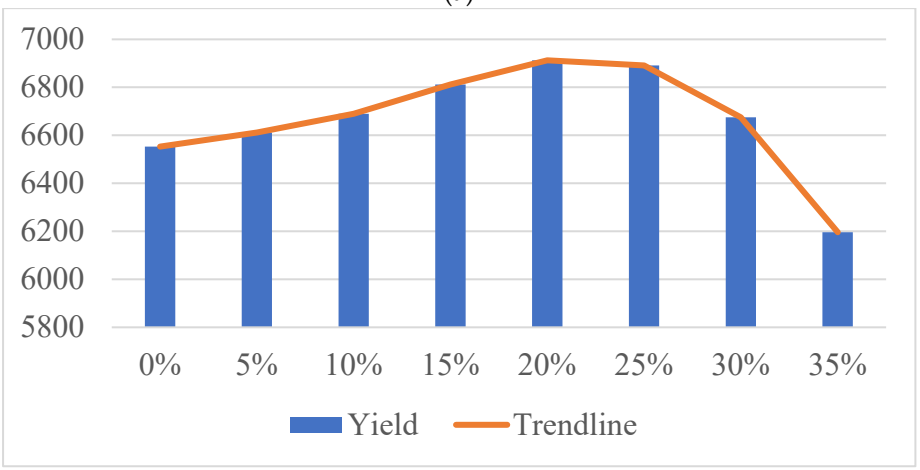

(**b**)

Figure 10. (**a**) Simulated results of final yield with different pruning intensities (Alaer). (**b**) Trends in simulated final yield with different pruning intensities (Alaer) based on modified model.

3.4. Simulated LAI under Different Pruning Intensities

The simulated results of LAI with different pruning degrees are shown in Figure 11. At pruning intensities below 15%, LAI changed little in the late growth season and the yield showed a trend of gradual increase. However, the yield was slightly less than 20% and 25% pruning. The reason may be that the smaller amount of pruning led to higher canopy closure, thereby reducing canopy light interception. When the pruning intensity was between 15% and 25%, the LAI changed drastically, which was due to the reduction in LAI caused by the large reduction in the number of canopy leaves. However, the appropriate pruning also improved the light interception capacity of the canopy, resulting in a lower extinction coefficient, enhanced photosynthesis, and increased light energy-use efficiency, which, in turn, increased the yield of fruit trees. With the increase in pruning intensity (more than 25%), the optimal balance of canopy light interception was broken, and the change in the extinction coefficient was no longer enough to influence the change in yield; therefore, the degree of its influence on yield decreased. At this point, the number of leaves played a decisive role in the overall photosynthesis of the canopy.

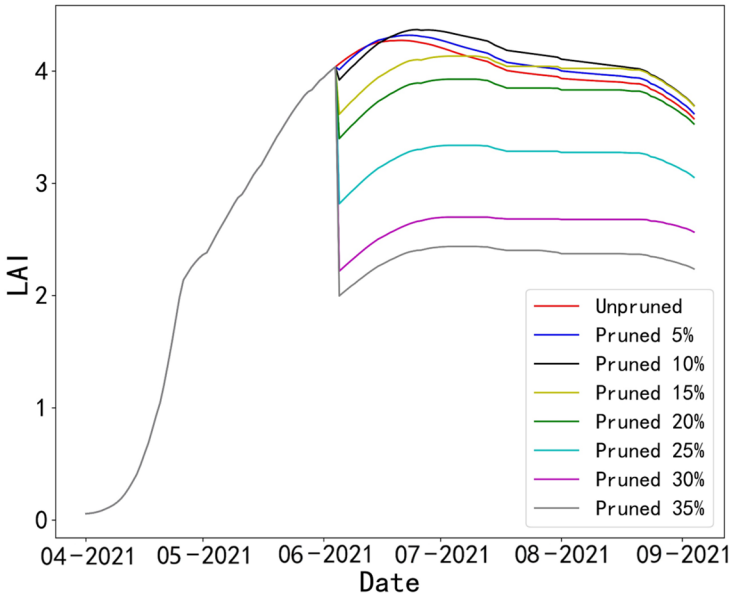

Figure 11. Results of LAI simulated under different pruning intensities (Alaer) based on modified model.

4. Discussion

4.1. Performance of the Improved Model in Pear Tree Growth Simulation and Soil Moisturre Assessment

In this study, the summer pruning process was considered, and the simulation performance of the model was effectively improved by modifying the WOFOST model with the calibrated parameters. It can be seen from Figure 6a,b and Figure 7a,b that the simulated results for TWSO and LAI before and after the model modification are acceptable. The model had better simulation results after the modification. The results indicate that it is feasible to simulate pear tree growth using the WOFOST model, and the modified model can further simulate the summer pruning process of pear trees and obtain a better fit with the actual observation. The improved model expresses growth simulations under water-limited conditions, which further strengthens the crop model's application in areas with water scarcity.

In this study, the same irrigation scheme was used for field trials and model inputs in both orchards. As can be seen from Figures 6c and 7c, the simulated results for soil water content from May to July were better fitted, while the simulated results for late August were underestimated because the pear orchard needed to be weeded before harvest and the pear orchard was rototilled, resulting in greater soil evaporation. The effect of different irrigation methods on the simulation results was not considered in this study. However, a previous study [2] showed that the effect of different irrigation treatments on the fruit development rate of pear trees would show up during the rapid fruit expansion period. In practice, different irrigation methods can affect the developmental stage and yield of pear trees [55]. The main reason for this is that water is the main component of photosynthesis, and different irrigation methods lead to different amounts of water being taken up by the roots from the soil, which, in turn, affects photosynthesis and the accumulation of organic matter.

4.2. Model Modification and Calibration

Modification and calibration of the crop model can improve the model's applicability. For example, the modified APSIM model could help to estimate the relative effect of alternative management practices under fluctuating high water tables [56], modified SWAP can accommodate the application of film mulching [57], a modified Kc model could reasonably predict crop evapotranspiration for flooded rice and winter wheat [58], and a modified

CERES-Maize model can simulate crop response to irrigation with saline water in Mediterranean conditions [59]. In this study, the modification of the WOFOST model is based on the simplification of the summer pruning process by splitting the summer pruning into leaf removal, stem removal and fruit removal, which facilitates the representation in the model. Note that the modified WOFOST model was calibrated against our experimental pear orchard and should be further validated in other areas to improve its applicability and reliability.

4.3. Model Modification Analysis Considering Pruning

The most fundamental purpose of summer pruning is to improve the canopy light interception structure, different pruning intensities mainly affect the diffuse visible extinction coefficient (KDIFTB), and adjusting the KDIFTB parameter can improve the model simulation accuracy. The value of KDIFTB decreases with increasing pruning intensity, and the distribution of light energy interception in the canopy improves, increasing photosynthesis and, thus, yield. The change in yield increases and then decreases with increasing pruning intensity, which is consistent with the results of the previous study [60]. In this study, the simulation accuracy of LAI and TWSO is effectively improved by adjusting KDIFTB according to the summer pruning intensity.

Since pruning is used to limit the lateral expansion of branches, summer pruning reduces both the LAI of the orchard and the size of the trees, thus reducing light interception, but improving the light environment for the fruit [16]. As shown in Figure 11, the LAI keeps growing smaller with increasing summer pruning intensity, but the magnitude of its change is inconsistent. At pruning intensities below 20%, the magnitude of LAI variation is small, and when the pruning intensity is greater than 20%, the magnitude of LAI variation increases. Pruning strategies vary from region to region, and the pruning of pear trees cultivated in the tropics should be mild [61]. The effects of pruning time nodes in summer on the phenological development and yield of pear trees can be verified by subsequent experiments. Compared with previous studies [49], the modified WOFOST model used to simulate the summer pruning process better represents the actual growth dynamics in the orchard.

A previous study [62] has shown that pruning affects transpiration, which has important implications for irrigation management in arid areas. At the annual growth scale, pruning during fruit expansion reduces transpiration water consumption and, within a certain range, increased pruning intensity reduces water consumption, thus improving fruit water use efficiency [63]. In arid areas, the pruning of fruit trees can effectively control water loss caused by transpiration, which affects the overall evapotranspiration of pear orchards. A previous study [19] has shown that moderate (25%) and heavy pruning (40%) obviously reduced transpiration and increased soil water content in dryland apples during the growing season. As the intensity of pruning increases, plant transpiration decreases.

The summer pruning in early June occurs in the early stage of slow fruit development, when the number of pear trees with hanging fruit has reached its peak, and the sizes of different fruits have visible differences. In practice, the smaller and scarred fruits should be removed, which can not only reduce the risk of fruit dropping due to weight, but can also concentrate the supply of nutrients to the larger individual fruit, improving the fruit quality. In the summer pruning of pear trees, pear varieties with more branches may need more pruning because of poor ventilation and light transmission. The pruning intensity requirements of different tree forms also varies greatly, depending on the light conditions of the tree form itself.

4.4. Effect of Meteorological Differences on the Yield of Pear Orchards

From Figures 9 and 10, it can be seen that the yield of the Alaer pear orchard is higher than that of Awat, while the planting management pattern of both orchards is almost the same. The main reason for this difference in yield is the difference in the meteorological conditions of local pear orchards. Photosynthesis in pear trees is sensitive to heat [64]. As

can be seen in Figure 5a, after the budding of pear trees and until the fruit-harvesting stage, the temperature increased and then continued to fluctuate at around 35 degrees Celsius. During the bud differentiation stage in mid-April, the temperature of Awat was higher than that of Alaer, and excessive temperature inhibits the bud differentiation, which, in turn, reduces the fruit's set rate. In mid-July, after the rapid expansion of fruits, the temperature of Awat was higher than that of Alaer, which affects the activity of the conversion enzymes in plants and reduces photosynthesis [65] while accelerating respiration and strengthening transpiration, resulting in less organic matter accumulation and lower yield. As shown in Figure 5b, the solar radiation intensity of Awat was higher than that of Alaer during the fruit development stage, and photosynthesis becomes stronger as the intensity increases within a certain solar radiation intensity. However, when the solar radiation is too strong, it destroys the protoplasm and causes chlorophyll decomposition [66], causes the cells of leaves lose too much water and close the stomata, or even causes cell death, resulting in weakened photosynthesis and a lower yield. Increased temperatures may negatively impact pear production through sunburn and heat stress [67]. Sunburn damage is more likely to occur in high-density orchards such as pear orchards, where UV radiation and direct sunlight heat the fruit surface, thereby damaging the fruit crop [68]. These will affect the yield of the pear orchard. In this study, the calibrated model responds well to the effects of meteorological changes (temperature and radiation) on yield, and the simulated yield is consistent with the measured value. However, it could not respond to the effects of heat stress and low-temperature stress on pear growth and yield.

4.5. Limitations of the Modified Model and Future Research Prospects

Pears have numerous varieties, and there are certain differences between different varieties [69]. Fruit tree variety differences may affect the accuracy of crop model yield estimations. In this study, only the dwarf, densely planted Korla pear was used as the study object, and no attention was paid to other varieties. Dwarf cultivars tend to have higher planting densities, so better canopy management strategies are needed to offset the negative effects of these high planting densities [70]. Further studies will focus on the effects of crop varieties and planting densities to improve the simulation accuracy of crop models.

Among the crop growth models that are commonly used at present, each has its own strengths and focus to meet the needs of different application directions [23,24]. Therefore, integrating the advantages of multiple crop models may further improve the accuracy of crop growth models [71,72]. At the same time, although crop models are calibrated and can perform acceptable field simulations, crop models may perform poorly when used to estimate regional crop yields, because it is often difficult to gather crop input information or parametric region-scale models. In these cases, remote sensing data assimilation strategies may be a promising way to deal with uncertain crop yield estimates [73].

A previous study [74] shows that an appropriate level of water deficit can improve water use efficiency by maintaining or slightly increasing fruit yield with reduced irrigation requirements. Additionally, the water deficit treatment shortens the fruit-ripening period and increases the economic value of the fruit [75]. The water gradient experiment in this study was not designed, and the effect of different irrigation treatments on yield was not analyzed. This should be considered in subsequent studies.

Weed roots in orchards penetrate the soil to absorb large amounts of water, as well as nutrients, which, when there are enough weeds in an orchard, can lead to serious malnutrition, slow growth, lower quality and lower yields [76,77]. Taller weeds tend to affect the sunlight that reaches fruit trees, especially climbing weeds and weeds that enter the canopy at a high level, which will reduce the light area of fruit tree leaves and thus reduce the photosynthetic strength of the plant, seriously affecting normal growth and development and fruit quality [78]. Considering how orchard weeds affect fruit tree growth is another important direction for future fruit tree growth model development.

5. Conclusions

This study focused on improving the WOFOST model to simulate the seasonal dynamic growth process of pear trees and soil moisture. According to the actual situation of the pear pruning operation, the WOFOST model was modified to be able to simulate the pear pruning process. After the experimental design and data collection calibration, the parameters that can simulate the growth of pear trees were obtained, and the growth and development of the annual growth cycle of pear trees was accurately simulated. The modified WOFOST model showed a better performance than the unmodified model in the simulation of TWSO (12.19% $\leq$ NRMSE $\leq$ 26.11%), LAI (NRMSE $\leq$ 10%) and SM (NRMSE $\leq$ 7.47%) under different pruning intensities. The modified WOFOST model can respond to summer pruning effects on pear orchard yield, total biomass and LAI. In sum, the proposed method is a potential way to analyze the effects of soil, meteorology, irrigation and pruning on fruit tree growth and water transport. In future research, the improvement in canopy light energy interception calculation methods and the development of remote sensing assimilation technology to reduce the uncertainty of model area-scale simulation may be crucial to improve the accuracy of fruit tree growth simulation.

Author Contributions: C.W. and N.Z. co-first author. C.W. wrote the manuscript. N.Z. drafted the outline and edited the manuscript. M.L. and L.L. analyzed data and validated the improved model. T.B. proposed the idea as supervisor. All authors have read and agreed to the published version of the manuscript.

Funding: This research was supported by "National Natural Science Foundation of China (62261046)", "Bingtuan Science and Technology Program (2021DB001, 2021BB023)" and "Graduate Scientific Research Innovation project of Tarim University, grant number (XJ2021G304)".

Institutional Review Board Statement: Not applicable.

Informed Consent Statement: Not applicable.

Data Availability Statement: Data from this study are not publicly available.

Conflicts of Interest: The authors declare no conflict of interest.

Appendix A

Table A1. Input main soil parameters for two orchards.

Input Main Soil Parameters	Description	Value (Alaer)	Value (Awat)
SMW	Soil moisture content at wilting point [cm^3/cm^3]	0.074	0.075
SMFCF	Soil moisture content at field capacity [cm^3/cm^3]	0.329	0.324
SM0	Soil moisture content at saturation [cm^3/cm^3]	0.410	0.410
K0	Hydraulic conductivity of saturated soil [cm day^{-1}]	23.97	23.85
SOPE	Maximum percolation rate root zone [cm day^{-1}]	1.37	1.41
KSUB	Maximum percolation rate subsoil [cm day^{-1}]	2.03	2.05
SMATB	Soil moisture content as function of pF [log (cm); cm^3 cm^{-3}]	Measured soil water retention (as function of pF)	Measured soil water retention (as function of pF)
CONTB	hydraulic conductivity as function of pF	Measured hydraulic conductivity	Measured hydraulic conductivity

Appendix B

Table A2. Main crop parameters used in WOFOST model for pear tree growth simulation.

Calibrated Crop Parameters	Description	Value	Units
TBASEM	Base temperature for emergence	10	°C
TEFFMX	Maximum effective temperature for emergence	30	°C
TSUMEM	Temperature sum from sowing to emergence	100	°C
TSUM1	Temperature sum from emergence to anthesis	140	°C d^{-1}
TSUM2	Temperature sum from anthesis to maturity	1880	°C d^{-1}
DTMSTB	Daily increase in temperature sum as a function of daily mean temperature	(0−10−35.5−40 °C) = 0.0−0.0−25.5−25.5 °C d^{-1}	°C d^{-1}
TDWI	Initial total crop dry weight	41.9	kg ha^{-1}
LAIEM	LAI at emergence	0.0007	ha ha^{-1}
RGRLAI	Maximum relative increase in LAI	0.060	ha ha^{-1} d^{-1}
SLATB	Specific leaf area as a function of DVS	(0.0−0.55−1.0−2.0) = 0.0020−0.0018-0.0016−0.0016 ha kg^{-1}	ha kg^{-1}
SPAN	Life span of leaves growing at 35 Celsius	85	[days]
TBASE	Lower threshold temp. for ageing of leaves	10.0	°C
KDIFTB	Extinction coefficient for diffuse visible light as function of DVS	(0.0−1.260−1.261-2.0) = 0.46−0.83−0.69−0.79	-
EFFTB	Initial light-use efficiency of CO_2 assimilation of single leaves as function of daily temperature	(19.5, 36.0) = 0.53−0.53	kg ha^{-1} hr^{-1} J^{-1} m^2 s
AMAXTB	Maximum leaf CO_2 assimilation rate as a function of development stage of the crop	(0.0, 1.6, 2.0) = 39.0−43.0−24.0	kg ha^{-1} hr^{-1}
TMPFTB	Reduction factor of AMAX as function of daily mean temperature	(10−19.5−35.5−40) = 0−1−1−0	-
CVL	Conversion efficiency of assimilates into leaf	0.73	kg kg^{-1}
CVO	Conversion efficiency of assimilates into storage organ	0.72	kg kg^{-1}
CVR	Conversion efficiency of assimilates into root	0.690	kg kg^{-1}
CVS	Conversion efficiency of assimilates into stem	0.65	kg kg^{-1}
Q10	Relative increase in maintenance respiration rate with each 10 degrees increase in temperature	2.0	-
RML	Relative maintenance respiration rate for leaves	0.0350	-
RMO	Relative maintenance respiration rate for storage organs	0.0130	-
RMR	Relative maintenance respiration rate for roots	0.0120	-
RMS	Relative maintenance respiration rate for stems	0.0100	-
FRTB	Fraction of total dry matter increase partitioned to roots as a function of development stage	(0.0−1.57−2.0) = 0.3−0.0−0.0	kg kg^{-1}
FLTB	Fraction of above ground dry matter increase partitioned to leaves as a function of development stage	(0.00−0.34−0.51−0.97−1.00−1.50−1.80−2.00) = 0.95−0.90−0.85−0.60−0.20−0−0−0	kg kg^{-1}
FSTB	Fraction of above ground dry matter increase partitioned to stems as a function of development stage	(0.00−0.34−0.51−0.97−1.00−1.50−1.80−2.00) = 0.05−0.10−0.15−0.40−0.70−0.75−0.10−0	kg kg^{-1}
FOTB	Fraction of above ground dry matter increase partitioned to storage organs as a function of development stage	(0.00−0.34−0.51−0.97−1.00−1.50−1.80−2.00) = 0.0−0.0−0.0−0.0−0.10−0.25−0.90−1	kg kg^{-1}

Table A2. *Cont.*

Calibrated Crop Parameters	Description	Value	Units
PERDL	Maximum relative death rate of leaves due to water stress	0.03	-
RDRSTB	Relative death rate of stems as a function of development stage	(0.0−1.0−1.5−2.0) = 0−0−0.02−0.02	-
CFET	Correction factor for potential transpiration rate	1.02	-
DEPNR	Dependency number for crop sensitivity to soil moisture stress	1.5	-
RDI	Initial rooting depth	10	cm
RRI	Daily increase in rooting depth	1.2	cm d^{-1}
RDMCR	Maximum rooting depth of the crop	120	cm

References

1. Wu, J.; Wang, Y.; Xu, J.; Korban, S.S.; Fei, Z.; Tao, S.; Ming, R.; Tai, S.; Khan, A.M.; Postman, J.D.; et al. Diversification and Independent Domestication of Asian and European Pears. *Genome Biol.* **2018**, *19*, 77. [CrossRef] [PubMed]
2. Wu, Y.; Zhao, Z.; Wang, W.; Ma, Y.; Huang, X. Yield and Growth of Mature Pear Trees under Water Deficit during Slow Fruit Growth Stages in Sparse Planting Orchard. *Sci. Hortic.* **2013**, *164*, 189–195. [CrossRef]
3. Zhao, Z.; Wang, W.; Wu, Y.; Xu, M.; Huang, X.; Ma, Y.; Ren, D. Leaf Physiological Responses of Mature Pear Trees to Regulated Deficit Irrigation in Field Conditions under Desert Climate. *Sci. Hortic.* **2015**, *187*, 122–130. [CrossRef]
4. Wu, Y.; Sun, M.; Liu, J.; Wang, W.; Liu, S. Fertilizer and Soil Nitrogen Utilization of Pear Trees as Affected by the Timing of Split Fertilizer Application in Rain-Fed Orchard. *Sci. Hortic.* **2019**, *252*, 363–369. [CrossRef]
5. Colpaert, B.; Steppe, K.; Gomand, A.; Vanhoutte, B.; Remy, S.; Boeckx, P. Experimental Approach to Assess Fertilizer Nitrogen Use, Distribution, and Loss in Pear Fruit Trees. *Plant Physiol. Biochem.* **2021**, *165*, 207–216. [CrossRef]
6. Hallgren, S.W. Tree Physiology | Shoot Growth and Canopy Development. *Encycl. For. Sci.* **2004**, 1600–1606. [CrossRef]
7. Persello, S.; Grechi, I.; Boudon, F.; Normand, F. Nature Abhors a Vacuum: Deciphering the Vegetative Reaction of the Mango Tree to Pruning. *Eur. J. Agron.* **2019**, *104*, 85–96. [CrossRef]
8. Kumar, M.; Rawat, V.; Rawat, J.M.S.; Tomar, Y.K. Effect of Pruning Intensity on Peach Yield and Fruit Quality. *Sci. Hortic.* **2010**, *125*, 218–221. [CrossRef]
9. Doll, U.; Mosqueira, D.; Mosqueira, J.; González, B.; Vogel, H. Pruning Maqui (Aristotelia Chilensis (Molina) Stuntz) to Optimize Fruit Production. *J. Appl. Res. Med. Aromat. Plants* **2017**, *6*, 10–14. [CrossRef]
10. Hampson, C.R.; Quamme, H.A.; Brownlee, R.T. Canopy Growth, Yield, and Fruit Quality of "Royal Gala" Apple Trees Grown for Eight Years in Five Tree Training Systems. *HortScience* **2002**, *37*, 627–631. [CrossRef]
11. Passos, L.C.; da Silva, J.R.; Rodrigues, W.P.; de Reis, F.O.; da Vasconcellos, M.A.S.; Machado Filho, J.A.; Campostrini, E. Leaf Photosynthetic Responses of Passion Fruit Genotypes to Varying Sunlight Exposure within the Canopies. *Exp. Plant. Physiol.* **2018**, *30*, 103–112. [CrossRef]
12. Zhang, S.; Ma, K.; Chen, L. Response of Photosynthetic Plasticity of Paeonia Suffruticosa to Changed Light Environments. *Env. Exp. Bot.* **2003**, *49*, 121–133. [CrossRef]
13. Li, Y.; Xin, G.; Wei, M.; Shi, Q.; Yang, F.; Wang, X. Carbohydrate Accumulation and Sucrose Metabolism Responses in Tomato Seedling Leaves When Subjected to Different Light Qualities. *Sci. Hortic.* **2017**, *225*, 490–497. [CrossRef]
14. Vosnjak, M.; Mrzlic, D.; Usenik, V. Summer Pruning of Sweet Cherry: A Way to Control Sugar Content in Different Organs. *J. Sci. Food Agric.* **2022**, *102*, 1216–1224. [CrossRef]
15. Mierowska, A.; Keutgen, N.; Huysamer, M.; Smith, V. Photosynthetic Acclimation of Apple Spur Leaves to Summer-Pruning. *Sci. Hortic.* **2002**, *92*, 9–27. [CrossRef]
16. Palmer, J.W.; Avery, D.J.; Wertheim, S.J. Effect of Apple Tree Spacing and Summer Pruning on Leaf Area Distribution and Light Interception. *Sci. Hortic.* **1992**, *52*, 303–312. [CrossRef]
17. Schaffer, B.; Gaye, G.O. Effects of Pruning on Light Interception, Specific Leaf Density and Leaf Chlorophyll Content of Mango. *Sci. Hortic.* **1989**, *41*, 55–61. [CrossRef]
18. Di, D.; Delle, S.; Vegetali, P.; Suolo, D.; Ambiente, E.D.; Of, P.; Fruit, W.; Di, D.; Delle, S.; Vegetali, P.; et al. Basic Considerations about Pruning Deciduous Fruit Trees. In *Advances in Horticultural Science*; Firenze University Press: Firenze, Italy, 2019; Volume 25, pp. 129–204.
19. Ye, M.; Zhao, X.; Biswas, A.; Huo, G.; Yang, B.; Zou, Y.; Siddique, K.H.M.; Gao, X. Measurements and Modeling of Hydrological Responses to Summer Pruning in Dryland Apple Orchards. *J. Hydrol.* **2021**, *594*, 125651. [CrossRef]
20. Yin, X.; Struik, P.C.; Goudriaan, J. On the Needs for Combining Physiological Principles and Mathematics to Improve Crop Models. *Field Crops Res.* **2021**, *271*, 108254. [CrossRef]

21. Chenu, K.; Porter, J.R.; Martre, P.; Basso, B.; Chapman, S.C.; Ewert, F.; Bindi, M.; Asseng, S. Contribution of Crop Models to Adaptation in Wheat. *Trends Plant Sci.* **2017**, *22*, 472–490. [CrossRef]
22. Soltani, A.; Sinclair, T.R. Modeling Physiology of Crop Development, Growth and Yield. In *Modeling Physiology of Crop Development, Growth and Yield*; CABi Publishing: Wallingford, UK, 2012; pp. 1–322. [CrossRef]
23. Jin, X.; Kumar, L.; Li, Z.; Feng, H.; Xu, X.; Yang, G.; Wang, J. A Review of Data Assimilation of Remote Sensing and Crop Models. *Eur. J. Agron.* **2018**, *92*, 141–152. [CrossRef]
24. Huang, J.; Gómez-Dans, J.L.; Huang, H.; Ma, H.; Wu, Q.; Lewis, P.E.; Liang, S.; Chen, Z.; Xue, J.H.; Wu, Y.; et al. Assimilation of Remote Sensing into Crop Growth Models: Current Status and Perspectives. *Agric. Meteorol.* **2019**, *276–277*, 107609. [CrossRef]
25. Hoogenboom, G. Contribution of Agrometeorology to the Simulation of Crop Production and Its Applications. *Agric. Meteorol.* **2000**, *103*, 137–157. [CrossRef]
26. Matthews, R.; Stephens, W.; Hess, T.; Middleton, T.; Graves, A. Applications of Crop/Soil Simulation Models in Tropical Agricultural Systems. *Adv. Agron.* **2002**, *76*, 31–124. [CrossRef]
27. Jones, J.W.; Hoogenboom, G.; Porter, C.H.; Boote, K.J.; Batchelor, W.D.; Hunt, L.A.; Wilkens, P.W.; Singh, U.; Gijsman, A.J.; Ritchie, J.T. The DSSAT Cropping System Model. *Eur. J. Agron.* **2003**, *18*, 235–265. [CrossRef]
28. Bergez, J.E.; Raynal, H.; Launay, M.; Beaudoin, N.; Casellas, E.; Caubel, J.; Chabrier, P.; Coucheney, E.; Dury, J.; Garcia de Cortazar-Atauri, I.; et al. Evolution of the STICS Crop Model to Tackle New Environmental Issues: New Formalisms and Integration in the Modelling and Simulation Platform RECORD. *Environ. Model. Softw.* **2014**, *62*, 370–384. [CrossRef]
29. Vanuytrecht, E.; Raes, D.; Steduto, P.; Hsiao, T.C.; Fereres, E.; Heng, L.K.; Garcia Vila, M.; Mejias Moreno, P. AquaCrop: FAO's Crop Water Productivity and Yield Response Model. *Environ. Model. Softw.* **2014**, *62*, 351–360. [CrossRef]
30. de Wit, A.; Boogaard, H.; Fumagalli, D.; Janssen, S.; Knapen, R.; van Kraalingen, D.; Supit, I.; van der Wijngaart, R.; van Diepen, K. 25 Years of the WOFOST Cropping Systems Model. *Agric. Syst* **2019**, *168*, 154–167. [CrossRef]
31. Nendel, C.; Berg, M.; Kersebaum, K.C.; Mirschel, W.; Specka, X.; Wegehenkel, M.; Wenkel, K.O.; Wieland, R. The MONICA Model: Testing Predictability for Crop Growth, Soil Moisture and Nitrogen Dynamics. *Ecol. Model.* **2011**, *222*, 1614–1625. [CrossRef]
32. Brown, H.; Huth, N.; Holzworth, D. Crop Model Improvement in APSIM: Using Wheat as a Case Study. *Eur. J. Agron.* **2018**, *100*, 141–150. [CrossRef]
33. Ceglar, A.; van der Wijngaart, R.; de Wit, A.; Lecerf, R.; Boogaard, H.; Seguini, L.; van den Berg, M.; Toreti, A.; Zampieri, M.; Fumagalli, D.; et al. Improving WOFOST Model to Simulate Winter Wheat Phenology in Europe: Evaluation and Effects on Yield. *Agric. Syst.* **2019**, *168*, 168–180. [CrossRef]
34. Sandhu, R.; Irmak, S. Performance of AquaCrop Model in Simulating Maize Growth, Yield, and Evapotranspiration under Rainfed, Limited and Full Irrigation. *Agric. Water Manag.* **2019**, *223*, 105687. [CrossRef]
35. Xu, J.; Bai, W.; Li, Y.; Wang, H.; Yang, S.; Wei, Z. Modeling Rice Development and Field Water Balance Using AquaCrop Model under Drying-Wetting Cycle Condition in Eastern China. *Agric. Water Manag.* **2019**, *213*, 289–297. [CrossRef]
36. Wolf, J. Comparison of Two Potato Simulation Models under Climate Change. II. Application of Climate Change Scenarios. *Clim. Res.* **2002**, *21*, 187–198. [CrossRef]
37. Li, M.; Du, Y.; Zhang, F.; Fan, J.; Ning, Y.; Cheng, H.; Xiao, C. Modification of CSM-CROPGRO-Cotton Model for Simulating Cotton Growth and Yield under Various Deficit Irrigation Strategies. *Comput. Electron. Agric.* **2020**, *179*, 105843. [CrossRef]
38. Wang, Z.; Ye, L.; Jiang, J.; Fan, Y.; Zhang, X. Review of Application of EPIC Crop Growth Model. *Ecol. Model.* **2022**, *467*, 109952. [CrossRef]
39. Wang, Y.; Lv, J.; Wang, Y.; Sun, H.; Hannaford, J.; Su, Z.; Barker, L.J.; Qu, Y. Drought Risk Assessment of Spring Maize Based on APSIM Crop Model in Liaoning Province, China. *Int. J. Disaster Risk Reduct.* **2020**, *45*, 101483. [CrossRef]
40. Constantin, J.; le Bas, C.; Justes, E. Large-Scale Assessment of Optimal Emergence and Destruction Dates for Cover Crops to Reduce Nitrate Leaching in Temperate Conditions Using the STICS Soil–Crop Model. *Eur. J. Agron.* **2015**, *69*, 75–87. [CrossRef]
41. Bai, T.C.; Wang, T.; Zhang, N.N.; Chen, Y.Q.; Mercatoris, B. Growth Simulation and Yield Prediction for Perennial Jujube Fruit Tree by Integrating Age into the WOFOST Model. *J. Integr. Agric.* **2020**, *19*, 721–734. [CrossRef]
42. de Wit, A.J.W.; Boogaard, H.L.; Supit, I.; van den Berg, M. *System Description of the WOFOST 7.2 Cropping Systems Model*; WOFOST: Wageningen, The Netherlands, 2020; p. 120.
43. van Diepen, C.A.; Wolf, J.; van Keulen, H.; Rappoldt, C. WOFOST: A Simulation Model of Crop Production. *Soil Use Manag.* **1989**, *5*, 16–24. [CrossRef]
44. Van Ittersum, M.K.; Leffelaar, P.A.; Van Keulen, H.; Kropff, M.J.; Bastiaans, L.; Goudriaan, J. On Approaches and Applications of the Wageningen Crop Models. *Eur. J. Agron.* **2003**, *18*, 201–234. [CrossRef]
45. Bassu, S.; Fumagalli, D.; Toreti, A.; Ceglar, A.; Giunta, F.; Motzo, R.; Zajac, Z.; Niemeyer, S. Modelling Potential Maize Yield with Climate and Crop Conditions around Flowering. *Field Crops Res.* **2021**, *271*, 108226. [CrossRef]
46. Ogutu, G.E.O.; Franssen, W.H.P.; Supit, I.; Omondi, P.; Hutjes, R.W.A. Probabilistic Maize Yield Prediction over East Africa Using Dynamic Ensemble Seasonal Climate Forecasts. *Agric. Meteorol.* **2018**, *250–251*, 243–261. [CrossRef]
47. Huang, J.; Tian, L.; Liang, S.; Ma, H.; Becker-Reshef, I.; Huang, Y.; Su, W.; Zhang, X.; Zhu, D.; Wu, W. Improving Winter Wheat Yield Estimation by Assimilation of the Leaf Area Index from Landsat TM and MODIS Data into the WOFOST Model. *Agric. Meteorol.* **2015**, *204*, 106–121. [CrossRef]
48. De Wit, A. Available online: https://pcse.readthedocs.io/en/stable/ (accessed on 6 March 2021).

49. Bai, T.; Zhang, N.; Wang, T.; Wang, D.; Yu, C.; Meng, W.; Fei, H.; Chen, R.; Li, Y.; Zhou, B. Simulating on the Effects of Irrigation on Jujube Tree Growth, Evapotranspiration and Water Use Based on Crop Growth Model. *Agric. Water Manag.* **2021**, *243*, 106517. [CrossRef]
50. van Dam, J.; Groenendijk, P.; Hendriks, R.; Jacobs, C. *Alterra Report1649-Swap32 Theory Description and User Manual*; Alterra: Wageningen, The Netherlands, 2009.
51. Hao, S.; Ryu, D.; Western, A.; Perry, E.; Bogena, H.; Franssen, H.J.H. Performance of a Wheat Yield Prediction Model and Factors Influencing the Performance: A Review and Meta-Analysis. *Agric. Syst.* **2021**, *194*, 103278. [CrossRef]
52. Akumaga, U.; Tarhule, A.; Yusuf, A.A. Validation and Testing of the FAO AquaCrop Model under Different Levels of Nitrogen Fertilizer on Rainfed Maize in Nigeria, West Africa. *Agric. Meteorol.* **2017**, *232*, 225–234. [CrossRef]
53. Fleming, A.; Schenkel, F.S.; Chen, J.; Malchiodi, F.; Bonfatti, V.; Ali, R.A.; Mallard, B.; Corredig, M.; Miglior, F. Prediction of Milk Fatty Acid Content with Mid-Infrared Spectroscopy in Canadian Dairy Cattle Using Differently Distributed Model Development Sets. *J. Dairy Sci.* **2017**, *100*, 5073–5081. [CrossRef]
54. Wang, D.; Wang, C.; Xu, L.; Bai, T.; Yang, G. Simulating Growth and Evaluating the Regional Adaptability of Cotton Fields with Non-Film Mulching in Xinjiang. *Agriculture* **2022**, *12*, 895. [CrossRef]
55. Wang, L.; Wu, W.; Xiao, J.; Huang, Q.; Hu, Y. Effects of Different Drip Irrigation Modes on Water Use Efficiency of Pear Trees in Northern China. *Agric. Water Manag.* **2021**, *245*, 106660. [CrossRef]
56. Malone, R.W.; Huth, N.; Carberry, P.S.; Ma, L.; Kaspar, T.C.; Karlen, D.L.; Meade, T.; Kanwar, R.S.; Heilman, P. Evaluating and Predicting Agricultural Management Effects under Tile Drainage Using Modified APSIM. *Geoderma* **2007**, *140*, 310–322. [CrossRef]
57. Zhao, Y.; Mao, X.; Shukla, M.K. A Modified SWAP Model for Soil Water and Heat Dynamics and Seed–Maize Growth under Film Mulching. *Agric. Meteorol.* **2020**, *292–293*, 108127. [CrossRef]
58. Qiu, R.; Li, L.; Liu, C.; Wang, Z.; Zhang, B.; Liu, Z. Evapotranspiration Estimation Using a Modified Crop Coefficient Model in a Rotated Rice-Winter Wheat System. *Agric. Water Manag.* **2022**, *264*, 107501. [CrossRef]
59. Castrignanò, A.; Katerji, N.; Karam, F.; Mastrorilli, M.; Hamdy, A. A Modified Version of CERES-Maize Model for Predicting Crop Response to Salinity Stress. *Ecol. Model.* **1998**, *111*, 107–120. [CrossRef]
60. du Toit, E.S.; Sithole, J.; Vorster, J. Pruning Intensity Influences Growth, Flower and Fruit Development of Moringa Oleifera Lam. under Sub-Optimal Growing Conditions in Gauteng, South Africa. *S. Afr. J. Bot.* **2020**, *129*, 448–456. [CrossRef]
61. de Alcântara Barbosa, C.M.; Pio, R.; de Souza, F.B.M.; Bisi, R.B.; Bettiol Neto, J.E.; da Hora Farias, D. Phenological Evaluation for Determination of Pruning Strategies on Pear Trees in the Tropics. *Sci. Hortic.* **2018**, *240*, 326–332. [CrossRef]
62. Molina, A.J.; Aranda, X.; Llorens, P.; Galindo, A.; Biel, C. Sap Flow of a Wild Cherry Tree Plantation Growing under Mediterranean Conditions: Assessing the Role of Environmental Conditions on Canopy Conductance and the Effect of Branch Pruning on Water Productivity. *Agric. Water Manag.* **2019**, *218*, 222–233. [CrossRef]
63. Nie, Z.; Wang, X.; Wang, Y.; Ma, J.; Wei, X.; Chen, D. Effects of Pruning Intensity on Jujube Transpiration and Soil Moisture of Plantation in the Loess Plateau. *IOP Conf Ser. Earth Env. Sci.* **2017**, *52*, 012048. [CrossRef]
64. Greer, D.H.; Weedon, M.M. Modelling Photosynthetic Responses to Temperature of Grapevine (Vitis Vinifera Cv. Semillon) Leaves on Vines Grown in a Hot Climate. *Plant. Cell Env.* **2012**, *35*, 1050–1064. [CrossRef]
65. Crafts-Brandner, S.J.; Salvucci, M.E. Sensitivity of Photosynthesis in a C4 Plant, Maize, to Heat Stress. *Plant. Physiol.* **2002**, *129*, 1773–1780. [CrossRef]
66. Hasanuzzaman, M.; Nahar, K.; Alam, M.M.; Roychowdhury, R.; Fujita, M. Physiological, Biochemical, and Molecular Mechanisms of Heat Stress Tolerance in Plants. *Int. J. Mol. Sci.* **2013**, *14*, 9643–9684. [CrossRef] [PubMed]
67. Feng, Y.; Wei, J.; Zhang, G.; Sun, X.; Wang, W.; Wu, C.; Tang, M.; Gan, Z.; Xu, X.; Chen, S.; et al. Effects of Cooling Measures on 'Nijisseiki' Pear (Pyrus Pyrifolia) Tree Growth and Fruit Quality in the Hot Climate. *Sci. Hortic.* **2018**, *238*, 318–324. [CrossRef]
68. Schrader, L.; Sun, J.; Zhang, J.; Felicetti, D.; Tianz, J. Heat and Light-Induced Apple Skin Disorders: Causes and Prevention. *Acta Hortic.* **2008**, *772*, 51–58. [CrossRef]
69. Niu, Y.; Chen, X.; Zhou, W.; Li, W.; Zhao, S.; Nasir, M.; Dong, S.; Zhang, S.; Liao, K. Genetic Relationship between the 'Korla Fragrant Pear' and Local Pear Varieties in Xinjiang Based on Floral Organ Characteristics. *Sci. Hortic.* **2019**, *257*, 108621. [CrossRef]
70. Menzel, C.M.; le Lagadec, M.D. Can the Productivity of Mango Orchards Be Increased by Using High-Density Plantings? *Sci. Hortic.* **2017**, *219*, 222–263. [CrossRef]
71. Siad, S.M.; Iacobellis, V.; Zdruli, P.; Gioia, A.; Stavi, I.; Hoogenboom, G. A Review of Coupled Hydrologic and Crop Growth Models. *Agric. Water Manag.* **2019**, *224*, 105746. [CrossRef]
72. Chapagain, R.; Remenyi, T.A.; Harris, R.M.B.; Mohammed, C.L.; Huth, N.; Wallach, D.; Rezaei, E.E.; Ojeda, J.J. Decomposing Crop Model Uncertainty: A Systematic Review. *Field Crops Res.* **2022**, *279*, 108448. [CrossRef]
73. He, L.I.; Jiang, Z.W.; Chen, Z.X.; Ren, J.Q.; Bin, L.I. Hasituya Assimilation of Temporal-Spatial Leaf Area Index into the CERES-Wheat Model with Ensemble Kalman Filter and Uncertainty Assessment for Improving Winter Wheat Yield Estimation. *J. Integr. Agric.* **2017**, *16*, 2283–2299. [CrossRef]
74. Cui, N.; Du, T.; Li, F.; Tong, L.; Kang, S.; Wang, M.; Liu, X.; Li, Z. Response of Vegetative Growth and Fruit Development to Regulated Deficit Irrigation at Different Growth Stages of Pear-Jujube Tree. *Agric. Water Manag.* **2009**, *96*, 1237–1246. [CrossRef]
75. Cui, N.; Du, T.; Kang, S.; Li, F.; Zhang, J.; Wang, M.; Li, Z. Regulated Deficit Irrigation Improved Fruit Quality and Water Use Efficiency of Pear-Jujube Trees. *Agric. Water Manag.* **2008**, *95*, 489–497. [CrossRef]

76. Zhang, Y.; Wang, L.; Yuan, Y.; Xu, J.; Tu, C.; Fisk, C.; Zhang, W.; Chen, X.; Ritchie, D.; Hu, S. Irrigation and Weed Control Alter Soil Microbiology and Nutrient Availability in North Carolina Sandhill Peach Orchards. *Sci. Total Environ.* **2018**, *615*, 517–525. [CrossRef] [PubMed]
77. Paušič, A.; Tojnko, S.; Lešnik, M. Permanent, Undisturbed, in-Row Living Mulch: A Realistic Option to Replace Glyphosate-Dominated Chemical Weed Control in Intensive Pear Orchards. *Agric. Ecosyst. Environ.* **2021**, *318*, 107502. [CrossRef]
78. Hammermeister, A.M. Organic Weed Management in Perennial Fruits. *Sci. Hortic.* **2016**, *208*, 28–42. [CrossRef]